

Article

Equilibrium Moisture and Drying Kinetics Modelling of Macroalgae Species *Ulva ohnoi* and *Oedogonium intermedium*

Craig Walker¹, Andrew Cole², Elsa Antunes¹ and Madoc Sheehan^{1,*}

¹ College of Science and Engineering, James Cook University, Townsville 4811, Australia; craig.walker@my.jcu.edu.au (C.W.); elsa.antunes1@jcu.edu.au (E.A.)

² MACRO—The Centre for Macroalgal Resources and Biotechnology, College of Science and Engineering, James Cook University, Townsville 4811, Australia; andrew.cole3@jcu.edu.au

* Correspondence: Madoc.sheehan@jcu.edu.au; Tel.: +61-747-814-153

Received: 27 February 2020; Accepted: 15 June 2020; Published: 22 June 2020



Abstract: Algae-based products have applications in the food and pharmaceutical industries, bioremediation of waste streams and biofuel production. Drying has been recognised to constitute the largest energy cost in algae processing, yet there is limited data or modelling characterising the drying kinetics of macroalgae. This research modelled the equilibrium moisture content of two macroalgae species, *Ulva ohnoi*, a saltwater alga and *Oedogonium intermedium*, a freshwater alga. The Guggenheim–Anderson–de Boer model was found to best represent experimental equilibrium moisture contents. Drying rate curves obtained under both convective and radiative conditions were fitted to an analytical solution of Fick’s second law, including the modelled equilibrium moisture values. Effective diffusivity values for the two species are presented.

Keywords: macroalgae; drying rates; equilibrium moisture; diffusion modelling

1. Introduction

Algae have been identified as a renewable resource that can be utilised for a range of products such as fertilisers and animal feeds, human food supplements, nutraceuticals, specialty chemicals, and bioenergy [1–3]. Historically the majority of research has focused on the development of microalgae, which are small single-celled algae. However, the commercial development of microalgae has been limited to high-value niche applications due to the technical difficulties and cost of large-scale cultivation and dewatering [4]. More recently, research effort in bioprocessing has broadened to include macroalgae, which are large multicellular alga found in both marine and freshwater environments. Due to their larger size and ease of harvesting, macroalgae are well suited to large-scale outdoor cultivation.

Macroalgae have the capacity to complement existing industries and drive sustainability and circular economy objectives by utilising their waste nutrients and water, effectively creating a sustainable source of high-protein biomass from waste inputs [5,6]. Neveux et al. [7] found that a freshwater species of macroalgae, *Oedogonium intermedium* (Chlorophyta), had the highest biocrude yield of a range of species, using hydrothermal liquefaction. Zeraatkar et al. [8] performed a review of algae in bioremediation of heavy metals from wastewater, which concluded both macro- and micro-algae were suitable candidates. Castine et al. [9] considered the use of macroalgae to treat wastewater from aquaculture, including added value from algae products. An assessment of the potential for algae in bioremediation was performed by Lawton et al. [10], where the saltwater macroalga *Ulva ohnoi* (Chlorophyta) was found to have the highest growth rates of a range of local species. Several macroalgae species including *O. intermedium* and *Asparagopsis taxiformis* (Rhodophyta) have potential

for use as a supplement to livestock feed, leading to improved growth rates and lower livestock methane emissions [11,12].

A significant barrier to the development of industry based around macroalgal production is the design of energy efficient and well-controlled drying systems that can transition freshly harvested biomass into a product suitable for storage and transport. The drying step of a process was recognised as the single biggest energy usage for the processing of algal biomass, due to the large amounts of moisture requiring removal [13]. The drying step can constitute up to 70–75% of processing costs in some cases. As such, optimisation of this step would lead to the largest gain in efficiency for the overall process.

Drying models are an effective way to understand and define the drying process and design drying equipment for industry. Industrial drying equipment can be broadly divided into drying via radiative and convective heating methods, with convective drying typically faster. Diffusion-based modelling has been extensively used in literature to describe both convective and radiative drying of food and biomaterials. This has been through the fitting of theoretical models based on Fick's law of diffusion, or fitting moisture data to empirical models with mathematical formulations that are identical to the first term in the analytical solution to Fick's law of diffusion, such as the Henderson and Pabis model [14].

Many studies in the literature have used diffusion modelling approaches to successfully represent macroalgae drying [15–19]. Other drying studies utilising diffusion-based modelling of algae include several covering the drying kinetics of the microalga *Arthrospira platensis* (Cyanobacteria) [20,21]. The use of diffusion modelling of other materials such as fibre, fruit, and vegetables is widespread in the literature.

The theoretical method of modelling diffusion-based drying kinetics is based on Fick's second law of diffusion [22]. A commonly used analytical series solution to Fick's second law, adapted to apply to the drying of an infinite slab of constant thickness, was derived by Sherwood [23] and is shown in Equation (1).

$$MR = \frac{M - M_e}{M_0 - M_e} = \frac{8}{\pi^2} \sum_{n=0}^{\infty} \frac{1}{(2n+1)^2} \exp\left(- (2n+1)^2 \frac{\pi^2 D_e t}{4L^2}\right) \quad (1)$$

In the equation MR is the dimensionless moisture ratio, M , M_e , and M_0 are moisture contents (% dry basis) at current, equilibrium, and initial times respectively. L is the material thickness (m), D_e is effective diffusivity (m^2/s), and t is drying time (s).

M_e is another important parameter in modelling drying kinetics as it defines the limits to which a material can be dried, given the conditions of the surroundings. Its value is important for product preservation, packaging, and storage. The equilibrium moisture content depends on the material as well as the relative humidity and temperature of the surroundings. It is typically modelled using adaptations of gas surface adsorption models. Lemus et al. [24] studied the equilibrium moisture content of the red alga *Agarophyton chilense* (Rhodophyta) between 5 and 40 °C and between 10% and 95% relative humidity. Other equilibrium moisture studies of macroalgae include the brown alga *Fucus vesiculosus* and *Macrocystis pyrifera* (Ochrophyta, Phaeophyceae) [15,16]. The best-fit equations in equilibrium moisture studies are typically the Guggenheim–Anderson–de Boer (GAB) or Bruenauer–Emmett–Teller models [25]. In the GAB model (Equation (2)) A , B , and C are model constants, E_{RH} is the relative humidity as decimal and M_e is the equilibrium moisture content in % dry basis. As an equilibrium moisture model, the GAB model has been shown to well represent M_e values over relative humidities between 5% and 90% for a range of different biomaterials [26].

$$M_e = \frac{ABCE_{RH}}{(1 - BE_{RH})(1 - BE_{RH} + BCE_{RH})} \quad (2)$$

The aim of this work is to model experimentally determined equilibrium moisture contents over a range of temperature and relative humidity conditions for two previously undescribed but commercially

important macroalgae species, *U. ohnoi* and *O. intermedium*. In this work, diffusion modelling and critical model parameters (effective diffusivities and activation energy) are experimentally determined and used to compare radiative and convective drying. These values are essential to determine safe storage moisture content limits and for obtaining accurate drying rate models. These model parameters are compared to results for other macroalgae.

2. Experiments

The algal biomass used in this study was obtained from stock cultures sourced from the Marine and Aquaculture Research Facilities Unit (MARFU) at James Cook University in Townsville, Australia. The two species used in the study were *U. ohnoi* and *O. intermedium*. *U. ohnoi* is a saltwater alga that forms thin, roughly rectangular blades up to 10 cm wide, with the thickness of each blade being two cells wide. It was selected from a range of saltwater species based on its high growth rates and high biocrude yield as well as high resistance to bacterial ingress [27,28]. *O. intermedium* is a freshwater alga that forms single filaments one cell wide, which can significantly clump together when harvested. Both species have potential for use as livestock feed supplement [11,29].

In both kinetic and equilibrium tests, surface moisture was removed from the algae samples via use of lab-scale centrifuge (Koh-I-Noor Engineering Works, Punjab, Pakistan) at 2800 RPM. Algae samples were dewatered in the centrifuge until outlet moisture flow completely stopped, which provided a consistent starting point for the drying and equilibrium moisture trials. Nine dewatered subsamples of the algae were used to determine the initial moisture content (M0) and to evaluate consistency in the determination of moisture content following the dewatering step. Dry weights were obtained using a moisture analyser (MA-45, Sartorius AG, 37075 Goettingen, Germany) drying at 110 °C to ensure complete moisture removal. Average initial moisture content (following dewatering) and 95% confidence interval for *U. ohnoi* was 81.73% weight \pm 1.4% (relative), and 83.54% weight \pm 1.1% (relative) for *O. intermedium*. The low variance in these starting-point (dewatered) moisture contents demonstrated both consistency in the dewatering process and in the use of the MA-45 to obtain moisture content and dry basis algae mass values.

2.1. Equilibrium Moisture Content

The setup used for the equilibrium moisture experiments consists of twelve sealed containers fully immersed in a hot water bath to control internal temperature. Each container was 500 ml in volume and had a mesh platform suspended above a saturated salt solution filling a third of the container volume. At a given temperature, a saturated salt solution will achieve equilibrium with the air inside the container, giving a fixed humidity [30]. Temperature (T) and humidity (ERH) inside the sample containers were measured using a humidity probe (Center 313, Center Technology Corporation, Taipei, Taiwan). Fresh centrifuged algae samples weighing approximately 4 g each were placed on the mesh platforms inside each container. Excess salts were used as a visual indicator to ensure saturated solutions during each experiment. The solutions used (and their respective relative humidities) at equilibrium were lithium chloride (11%); sodium acetate (20%); magnesium chloride (31%); sodium carbonate (43%); and sodium bromide (52%). Three containers of each solution were used to obtain triplicate results for each temperature and humidity.

The mass of the algae samples was measured daily after being left for a week to reach equilibrium. Three consecutive and constant measurements were obtained to ensure equilibrium. The measured equilibrium masses were converted to moisture content in % dry basis via Equation (3);

$$M_e(\%db) = \left(\frac{M_{e,g} - D}{D} \right) \quad (3)$$

where $M_{e,g}$ is the equilibrium mass of the algae in grams, and D is the dry weight of the algae in grams. Algae dry weight was determined using the Sartorius MA-45.

2.2. Drying Kinetics

Freshly centrifuged algae was used to experimentally investigate drying kinetics. Given proteins in algae are prone to denaturation at high temperature, and characteristics such as colour also deteriorate (changing from green to brown) at high temperature, temperatures used for the experimental runs were 40, 50, and 60 °C. Three repeats were performed for each temperature. The initial material thickness ($L = 0.01$ m) and the initial fresh mass were kept constant between runs.

A Sartorius MA-45 moisture analyser was used for the radiation drying experiments. Relevant technical details for the moisture analyser are as follows: frequency 48–60 Hz, temperature range 40–230 °C in 1 °C increments, mass measurement accuracy of 0.2%, balance resolution 1 mg. Initial fresh masses were set at 1.5 g. Triplicates of moisture ratio versus time showed excellent consistency in experimental moisture profiles obtained under radiative drying conditions (Figure 1).

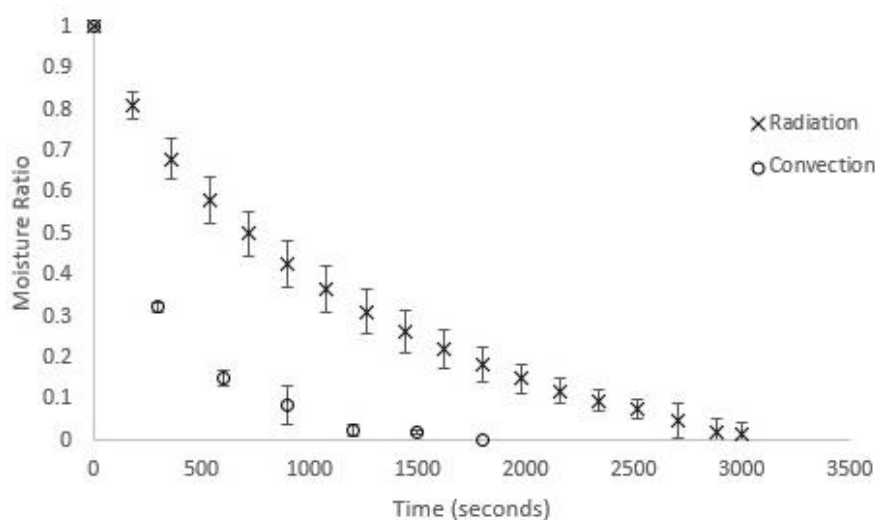


Figure 1. Triplicate moisture profiles for *U. ohnoi* at 40 °C for radiative and convective drying.

A convective food desiccator (Ezi-Dri FD-1000, Hydraflow Industries Limited, Upper Hutt, New Zealand) was used for the convection drying experiments. The equipment passes heated air through vertically stacked trays on which the algal material is placed. Gas temperature (40, 50, 60 °C) and flow rate (0.7 m/s) were confirmed from measurement of outlet conditions via hot-wire anemometer (AM-4214SD, Lutron Electronics Enterprise, Taipei, Taiwan). Initial biomass weight was measured before placement in the stacked trays. Trays were removed in a randomised order at discrete time intervals and material weight was obtained at each interval. Randomisation was chosen to reduce any potential effects of tray positions on the drying kinetics. Humidity of the exhaust air was measured directly using a handheld humidity meter and probe (Center 313, Center Technology Corp., Taipei, Taiwan). Initial fresh masses on each tray were set at 7 g.

2.3. Analysis Methods

2.3.1. Equilibrium Moisture

For each algae type, two equilibrium moisture content models (BET and GAB) were fitted to the experimentally determined equilibrium moisture content at each temperature and relative humidity. Model fitting was performed by adjusting model parameter values to minimise the total sum of square errors between the model and the triplicate experimental data sets. Initial guess values for the model fit process were chosen to represent the expected parameter range for the equations, and a wide range of different initial parameter values was tested to ensure the global minimum was found. These calculations were performed using Microsoft Excel using the solver function with GRG nonlinear

solver method. The objective function is summarised in Equation (4), where m corresponds to a given data set, and the objective function (Obj) is minimised by varying the model constants.

$$Obj = \sum_{m=1}^3 \left(\sum (M_{e,m} - M_{e,exp})^2 \right) \quad (4)$$

2.3.2. Drying Kinetics

The raw experimental data of mass against time in the convective and radiative drying experiments were converted to moisture ratio versus time. An analytical solution to the Fick's second law model (Equation (1)) was fitted to moisture ratio versus time data sets. Model fitting was performed by minimisation of the total sum of square errors between the model and experimental data, with the model representing the best fit to all three sets of data at a given condition. Ten terms of the infinite series were used in modelling to ensure convergence in the infinite series solution [31]. These calculations were performed using Microsoft Excel with the solver function and GRG nonlinear solver method, assuming constant relative variance in the experimental data. The objective function is summarised in Equation (5), where m corresponds to the number of data sets. The objective function (Obj) was minimised by varying the magnitude of the effective diffusivity parameter (D_e).

$$Obj = \sum_{m=1}^3 \left(\sum (MR_m - MR_e)^2 \right) \quad (5)$$

3. Results

3.1. Equilibrium Moisture Modelling

Of the models used, the best fit (i.e., demonstrating the highest R^2 value) for both species over the conditions tested was the GAB model. We recommend this model to be adopted for both species. The model constants and the goodness of fit (R^2) for the GAB equation are summarised in Table 1. Graphs of the experimental equilibrium moisture compared with the GAB model predictions are shown in Figure 2 for both species.

Table 1. Guggenheim–Anderson–de Boer (GAB) model coefficients and fit.

Algae	Temperature (°C)		
	35	45	55
<i>U. ohnoi</i>			
A	0.109	0.075	0.040
B	1.496	1.689	1.889
C	2.68×10^5	2.847×10^5	2.38×10^4
R^2	0.844	0.977	0.989
<i>O. intermedium</i>			
A	0.069	0.077	0.106
B	0.824	0.845	0.894
C	13.39	21.04	5.29
R^2	0.881	0.967	0.999

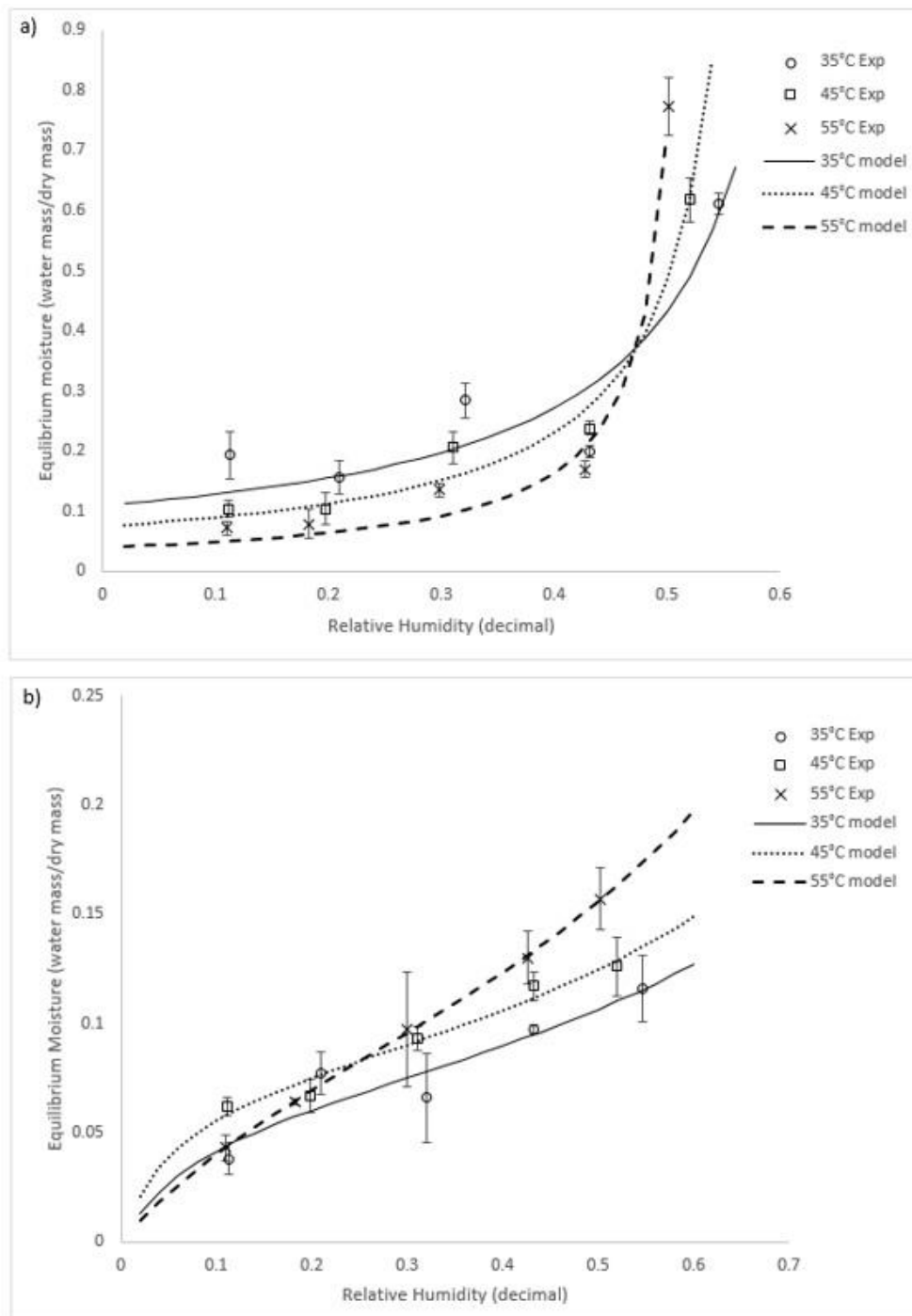


Figure 2. GAB model and experimental data for (a) *U. ohmoi* and (b) *O. intermedium* (Exp = experimental; model = modelling outcome).

A statistical analysis was performed using SPSS software to determine the significance of temperature and relative humidity for determining the equilibrium moisture. A general linear univariate model analysis was used, which provided regression and variance analysis of the equilibrium moisture as the dependent variable against temperature and relative humidity. The analysis showed that both temperature and relative humidity were statistically significant in their ability to predict changes in the equilibrium value for both species (significance < 0.05 for all variables for both species). F-tests (a measure of the relative predictive ability) showed that, of the two variables, relative humidity was the best single predictor of the equilibrium moisture content. Comparing between the two types

of algae, *U. ohnoi* exhibited a significantly higher equilibrium moisture content than *O. intermedium*. It is assumed that this was because *U. ohnoi* has reduced surface area (algal sheets are two cells thick rather than the single cell strings of *O. intermedium*) and is a saltwater alga.

At around 50% humidity for *Ulva* and 30% humidity for *O. intermedium*, there was a crossover point where higher temperatures resulted in higher equilibrium moisture than those observed at lower temperatures. Lemus et al. [24] had a similar crossover effect at higher humidities in a study of the red macroalga *Agarophyton chilense*, as did Moreira [15] for *Fucus vesiculosus*. They reasoned that this was due to solubility effects of polysaccharides and proteins that make up the majority of the alga solids mass. The crossover point would then be where these solubility effects on the equilibrium point become larger than effects of the surrounding atmospheric conditions. Similar results have been shown for other algae biomass, including *Gelidium corneum* (Rhodophyta), as well as other biomaterial with soluble components [32,33]. Both *U. ohnoi* and *O. intermedium* have polysaccharide and protein content totalling about 60% of dry mass [7]. It should be noted that the GAB equation is not designed to represent these interactions. As such, it follows that the parameters of the GAB equation are semi-empirical or empirical in this application, reinforcing the importance of experimental characterisation of algal species.

In general, equilibrium moisture isotherms and equilibrium moisture magnitudes for both species were similar to those for other macroalgae and biomaterials. Table 2 provides equilibrium moisture content values for this work and also for a variety of biomass types.

Table 2. Examples of equilibrium moisture contents for various biomaterials and algae.

Material	Temperature(°C)	Relative Humidity (%)	M_e (%db)
Apple [34]	45	20–90	4–81
Pear [34]	45	19–93	2–73
Argan (leaves) [35]	40	7–90	3–30
Canola [36]	40	10–90	4–10
<i>O. intermedium</i> [this study]	45	10–50	6–12
<i>U. ohnoi</i> [this study]	45	10–50	10–60
<i>Arthrospira platensis</i> [20]	30	5–90	4–40
<i>Fucus vesiculosus</i> [15]	45	10–70	2–70
<i>Macrocystis pyrifera</i> [16]	50	10–70	5–200
<i>Agarophyton chilense</i> [24]	40	10–80	0.5–100
<i>Gelidium corneum</i> [32]	40	10–90	5–40

3.2. Drying Kinetics Modelling

The model-predicted effective diffusivities for both *Ulva* and *O. intermedium* at each temperature were determined by including the GAB-modelled equilibrium moisture contents (M_e). The parameter-estimated effective diffusivities are shown in Table 3 for both species. The effective diffusivity was lower for *O. intermedium* than *U. ohnoi* and this is likely due to the tendency for *O. intermedium* to clump together when harvested, which reduces overall contact area for drying compared with individual blades of *U. ohnoi*.

Table 3. Effective diffusivity from radiative and convective drying.

Temperature (°C)	Radiative Heating: D_e (m ² /s)		Convective Heating (0.7 m/s): D_e (m ² /s)	
	<i>U. ohnoi</i>	<i>O. intermedium</i>	<i>U. ohnoi</i>	<i>O. intermedium</i>
40	3.18×10^{-8}	2.32×10^{-8}	1.17×10^{-7}	5.66×10^{-8}
50	5.47×10^{-8}	3.63×10^{-8}	1.40×10^{-7}	6.66×10^{-8}
60	8.75×10^{-8}	4.82×10^{-8}	1.48×10^{-7}	8.94×10^{-8}

Diffusivity values for the two species were similar to those of other macroalgae, summarised in Table 4. However, diffusivities for both algae species were high compared to those determined for microalgae drying. For example, effective diffusivities for spirulina drying under convective conditions were in the range 3×10^{-10} to 7×10^{-10} m²/s [21]. Both species of macroalgae had relatively high effective diffusivities compared to other biomaterials, such as wood and fruit slices, which indicates a lower internal resistance to diffusion for macroalgae. This was likely due to the comparative simplicity of the algae material combined with the large discrete particles giving a high void fraction. The algae cells also use diffusion across cell walls to transfer water and nutrients from their surroundings. This predisposition could be enhancing the drying rate in comparison to material like wood and fruits. Generally, biomaterials with comparatively lower effective diffusivities have outer solid surfaces (e.g., bark) that do not facilitate moisture transfer (to the same extent that algae does), as well as being materials with more complex structures (e.g., lignin, fibres) that include multiple different internal layers.

Table 4. Examples of effective diffusivity values for various biomaterials during convective drying.

Biomaterial	Temperature (°C)	Air Velocity (m/s)	Diffusivity (m ² /s)
Fig [37]	45–65	1–5	$3\text{--}16 \times 10^{-10}$
Persimmon [38]	50	0–12	$2.4\text{--}6 \times 10^{-10}$
<i>O. intermedium</i> [this study]	40–60	0.7	$5.7\text{--}8.9 \times 10^{-8}$
<i>U. ohnoi</i> [this study]	40–60	0.7	$1.2\text{--}1.5 \times 10^{-7}$
<i>Arthrospira platensis</i> [21]	40–60	0–1.2	$3.1\text{--}6.7 \times 10^{-10}$
<i>Durvillaea antarctica</i> [18]	40–80	1.5	$0.7\text{--}2.4 \times 10^{-9}$
<i>Fucus vesiculosus</i> [15]	35–75	2	$1\text{--}3 \times 10^{-10}$
<i>Himanthalia elongata</i> [19]	25–40	2	$5.6\text{--}12.2 \times 10^{-7}$
<i>Macrocystis pyrifera</i> [16]	50–80	2.1	$5.6\text{--}10.2 \times 10^{-9}$

Graphs of the experimental data for radiative and convective drying of both algae species are compared to each fitted model in Figures 3 and 4, respectively. The general fit of the Fick's second law model to the experimental data is excellent (R^2 values in all runs except for 40 °C radiative heating for *O. intermedium* were between 0.945 and 0.99). However, the model had a tendency to under-predict the experimental data for moisture ratios between one and 0.3, then over-predict as the moisture ratio approached zero. Worst fit was *O. intermedium* at 40 °C under radiation drying, where the tendency of the algal biomass to clump unevenly caused an increase in the variance of the experimental data. Convection drying rates were higher than for radiation, with increased heat transfer and slab penetration likely to be the cause.

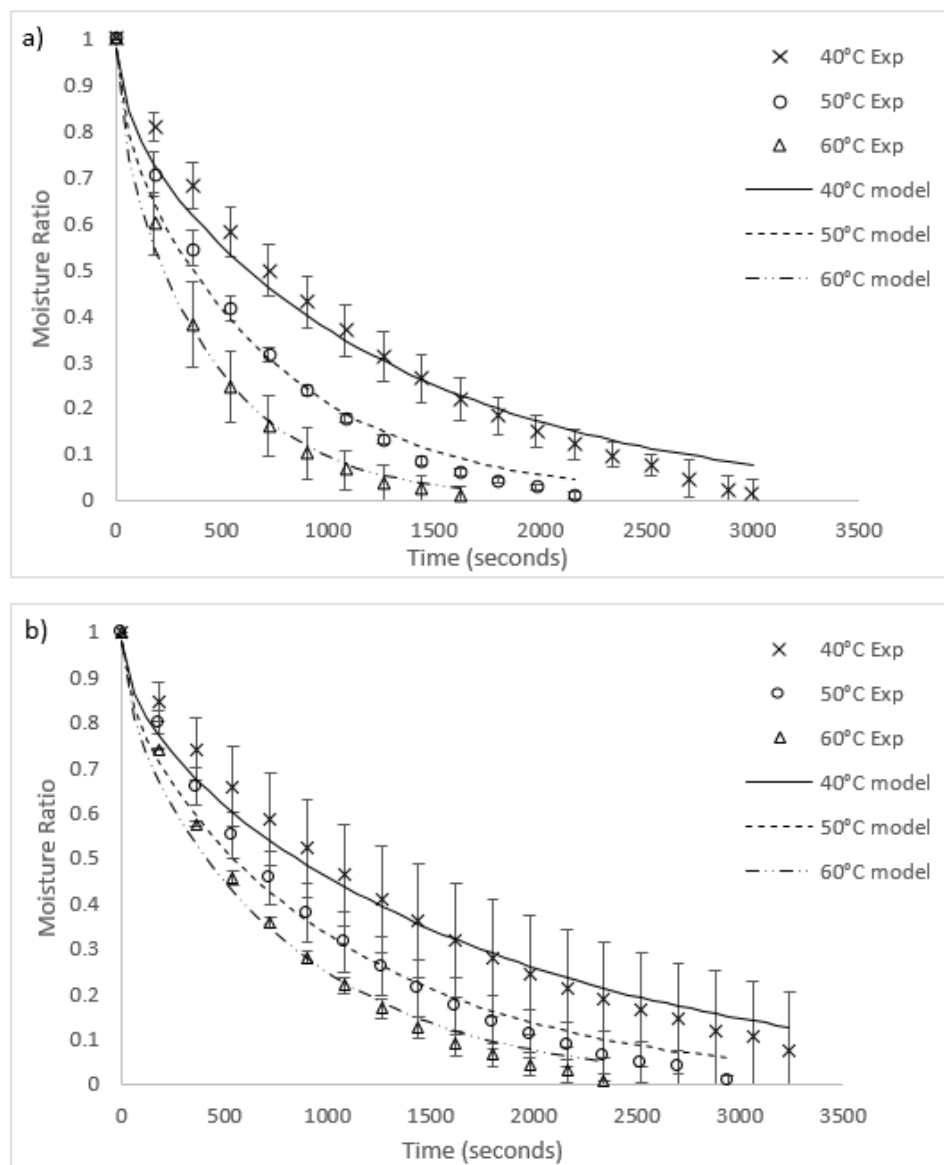


Figure 3. Comparison of radiation drying results and models for (a) *U. ohnoi* and (b) *O. intermedium* (Exp = experimental; model = modelling outcome).

The assumptions made in the derivation of this analytical solution are: initial moisture distribution is even; internal moisture transport is by diffusion only; drying gas volumes are large enough that surrounding environmental conditions are not changed by moisture transfer; slab thickness is constant throughout the drying process; temperature of the slab is isothermal and equal to the temperature of the surroundings; and bulk transfer of moisture (by convection) to the surroundings is sufficiently fast that drying is only limited by the internal rate of diffusion. These conditions are rarely if ever fully satisfied, and D_e is used in drying kinetics to pragmatically represent a global effective diffusivity, which accounts for these deviations. In this way, the diffusion coefficient consolidates the effects of deviations from these assumptions into a single (lumped) parameter model. This covers internal effects such as resistance to diffusion from material layers and a biomaterial's binding strength holding moisture internally, as well as external effects of temperature gradients, drying gas velocity and humidity. The effective diffusivity approach requires new experimental results for new materials, due to the influence of material properties. In the case of biomaterial drying there is typically some volume loss or material shrinkage that occurs, and there is also an initial heating period required to bring the biomaterial up to the gas temperature. Despite these physical and mechanistic deviations from ideal

behaviour, model accuracy remains typically high and any errors introduced by using this modelling approach are widely considered to be acceptable. Both materials undergo significant shrinkage during drying, which is not accounted for in the analytical model. This shrinking would reduce the effective slab thickness as the material dries, which would lead to increased effective diffusivity values as drying progresses. A solution of the original Fick's second law partial differential equations by including time-variant boundary conditions would be required to account for this effect. However, the complexity of this approach would limit its utility for industry practitioners seeking to use model equations to design drying operations.

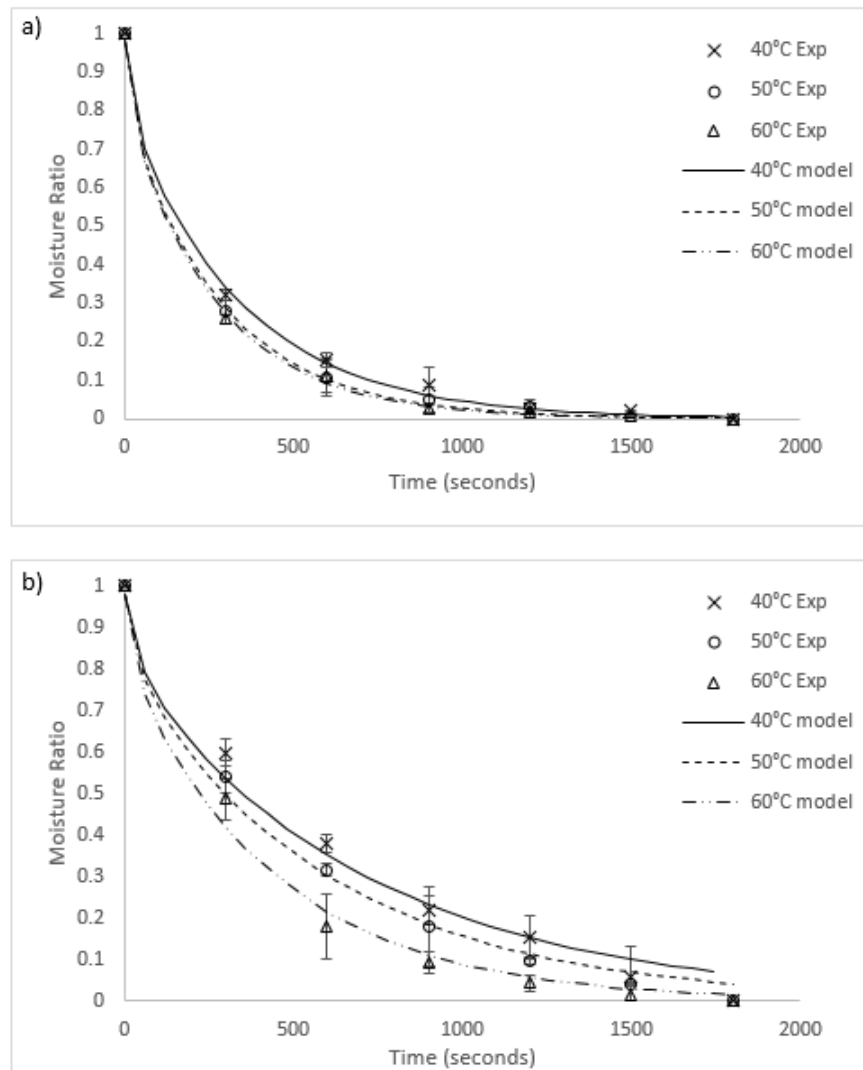


Figure 4. Comparison of convection drying results and models for (a) *U. ohnoi* and (b) *O. intermedium* (Exp = experimental; model = modelling outcome).

Radiative drying was measured as slower than convection drying. There are two potential explanations as to why this could be the case. The first is that drying was not a diffusion-limited process and was instead controlled by moisture removal at the surface. This would lead to accumulation of moisture on the surface, and result in constant-rate drying. This was investigated by numerically calculating the drying rate using second order Taylor approximation. Figure 5 includes graphs of the rate of change of drying for both algae species, shown as absolute values. In these graphs, a constant-rate drying period would show as a horizontal trend in the initial drying stage. The graphs in Figure 5 show that drying was in a single falling-rate period for both species and all temperatures.

The shape is the same as the expected rate of change from the Fick's law model. This shows the assumption of diffusion-limited drying is correct.

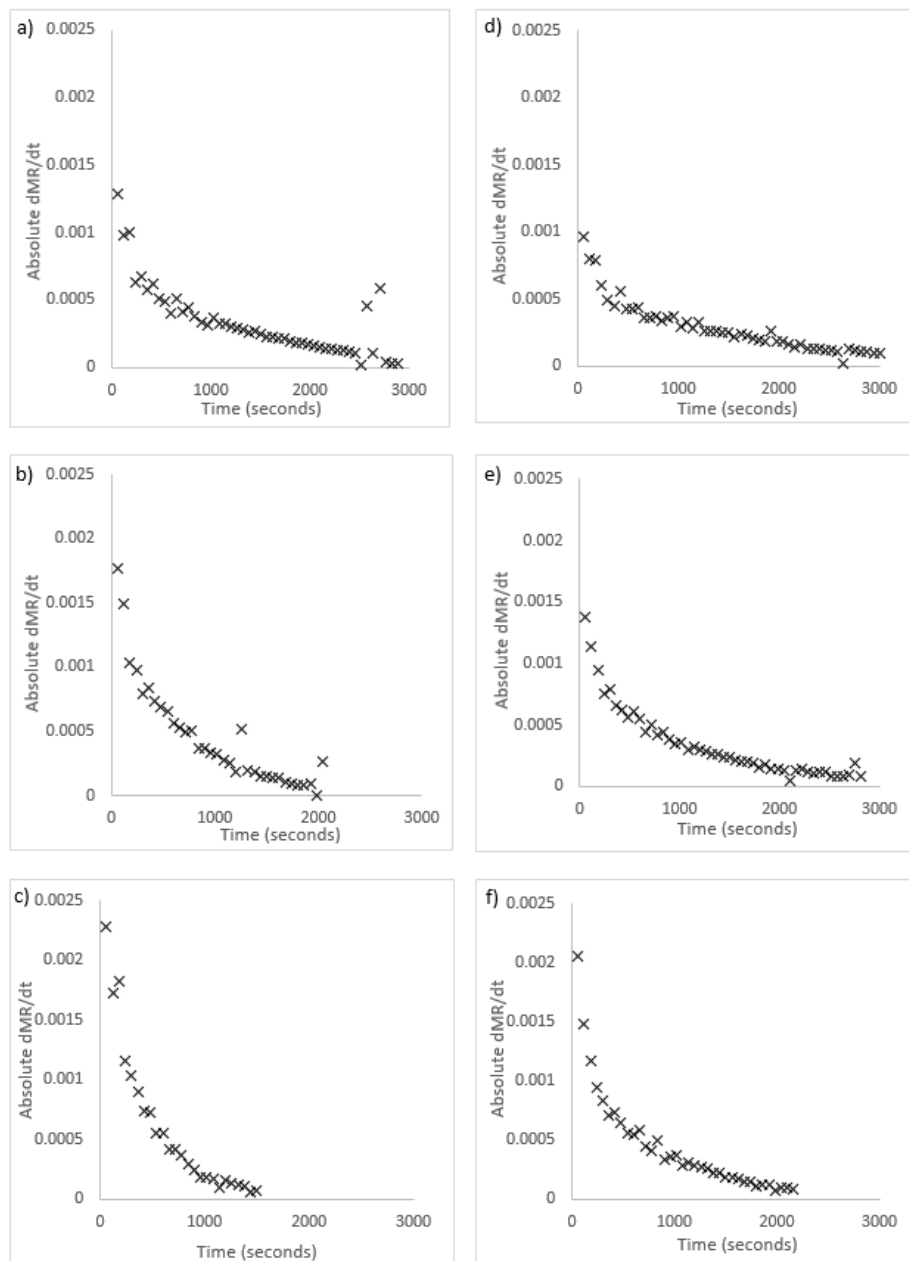


Figure 5. Dimensionless moisture ratio (MR) rate of change vs time for radiative drying; *U. ohnoi* (a) 40 °C (b) 50 °C (c) 60 °C; *O. intermedium* (d) 40 °C (e) 50 °C (f) 60 °C.

Given that diffusion-limited drying was occurring, the addition of air flow must then have been affecting the material in a way that led to an apparent increase in effective diffusivity. Several other studies have shown increases in air velocity cause an increase in effective diffusivity, including for eggplant, potato slices, and other macroalgae [17,39,40]. Other materials have been studied with results showing little to no effect with flow rate changes, including a selection of vegetables and a differently structured macroalga [32,41]. There is little discussion on possible mechanisms for this in literature. The most likely explanation is that airflow causes an increase in penetration through the material slab, which results in a reduction of the average distance moisture is required to diffuse through (i.e., the parameter L , the slab width reduces with increasing gas velocity). In this case, we are choosing a

pragmatic approach, leaving L as the initial slab width and representing the effect as an increase in the effective diffusivity. Comparing this work with other observations of the effect of convection indicates that materials composed of particulates or with porous structure show increased diffusivity with air flow, while those closer to solid slabs of material do not.

The Fick's law analytical model enables a mechanistic or theoretical description of the influence of temperature, through the determination of activation energy of drying. Studies of drying kinetics typically show temperature has an Arrhenius-type relationship to the effective diffusivity, shown in Equation (6);

$$D_e = D_0 \exp\left(-\frac{E_a}{RT}\right) \quad (6)$$

where D_0 is the diffusion pre-exponential factor (m^2/s), E_a is the activation energy (J/mol), R is the ideal gas constant ($8.314 \text{ J}/\text{mol}\cdot\text{K}$), and T is temperature in Kelvin.

Assuming this type of relationship holds true for diffusivity and temperature and no other compounding effects exist (for example, material degradation from high temperature), D_0 represents the effective diffusivity at an infinitely high temperature and E_a is the energy to overcome the "barrier" to diffusion. This barrier is the energy to overcome the initial moisture binding in the case of internally bound moisture in macroalgae and other biomaterials. These values were estimated by plotting the natural log of the parameter-estimated effective diffusivity versus $1/T$ from radiative drying trials (shown in Figure 6). The slope of the fitted line is then equivalent to $-E_a/R$, and the y-intercept is equivalent to $\ln(D_0)$. For a complete radiative drying model description, the recommended values of E_a and D_0 for both species are shown in Table 5. A comparison of the E_a values with literature results for other macroalgae and biomaterials is shown in Table 6. For convective drying at 0.7 m/s , it is recommended to use the diffusivity values (D_e) at the appropriate drying temperature, shown in Table 3.

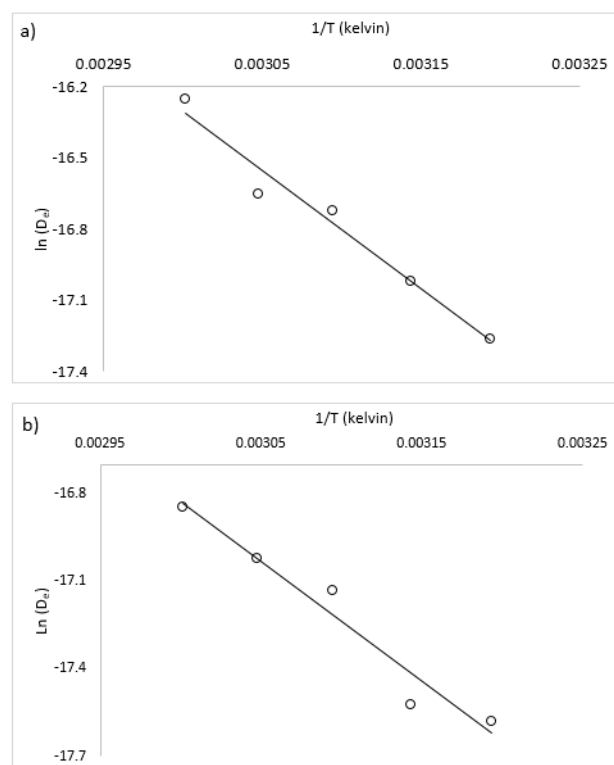


Figure 6. Graphical solution method for calculation of activation energy and diffusion pre-exponent, (a) *U. ohnoi* and (b) *O. intermedium*.

Table 5. Activation energy and diffusion pre-exponent for radiative drying.

Algae	E_a (kJ/mol)	D_0 (m ² /s)	R^2
<i>U. ohnoi</i>	41.3	0.24	0.968
<i>O. intermedium</i>	34.1	0.011	0.948

Table 6. Comparison of D_0 and E_a for other biomaterials.

Material	Activation Energy (kJ/mol)
Red pepper [42]	23.35
Orange seeds [43]	16.5
<i>Fucus vesiculosus</i> [15]	22.1
<i>Himantalia elongata</i> [19]	37.2
<i>Macrocystis pyrifera</i> [16]	25.31
<i>Agarophyton chilense</i> [24]	39.9

4. Conclusions

Important drying and moisture equilibrium properties of two commercially important macroalgae species were characterised in lab-based trials. The GAB moisture sorption model showed the best fit to experimentally determined equilibrium moisture contents for both *U. ohnoi* and *O. intermedium* macroalgae over industry-relevant temperature and relative humidity ranges (35–55 °C and 10–60% RH). Relative humidity was found to be the most significant variable in predicting equilibrium moisture content for both types of algae, and environmental limits for safe algae storage were clearly identified. An analytical solution to Fick's second law of diffusion was used to model both convective and radiative drying kinetics for both algae species with a high degree of correlation. Moisture ratio versus time data showed that drying for both species occurs in a falling-rate period at all times and temperatures (40–60 °C), indicating diffusion-limited drying and reinforcing the validity of the analytical model for these biomaterials. Convective drying at 0.7 m/s demonstrated an increased drying rate compared to radiative drying at the same temperature, reinforcing the value in gas-assisted drying technologies. Diffusion coefficients under both radiative and convective conditions, as well as activation energies, were determined for both species. These model parameters were compared to literature values for other biomaterials and showed consistency. Increased rates of diffusion under convective conditions were attributed to the drying gas flow penetrating into the material "slab" and reducing diffusion distance (i.e., slab thickness). Given the significant influence of gas velocity on the drying rates observed in this study, the effects of both gas velocity and material thickness should be more extensively investigated for both macro- and microalgae.

Author Contributions: Conceptualization, M.S.; methodology, C.W. and M.S.; formal analysis, C.W.; writing—original draft preparation, M.S. and C.W.; writing—review and editing, M.S., E.A., A.C.; supervision, M.S. and A.C. All authors have read and agreed to the published version of the manuscript.

Funding: This research received no external funding.

Acknowledgments: The algal biomass used in this research was supplied by Pacific Bio Pty Ltd. as part of their research and development program on algal bioremediation and bio-products.

Conflicts of Interest: The authors declare no conflict of interest.

References

1. Angell, A.; Angell, S.; de Nys, R.; Paul, N. Seaweed as a protein source for mono-gastric livestock. *Trends Food Sci. Technol.* **2016**, *54*, 74–84. [[CrossRef](#)]
2. Mabeau, S.; Fleurence, J. Seaweed in food products: Biochemical and nutritional aspects. *Trends Food Sci. Technol.* **1993**, *4*, 103–107. [[CrossRef](#)]

3. Garcia-Vaquero, M.; Hayes, M. Red and green macroalgae for fish and animal feed and human functional food development. *Food Rev. Int.* **2016**, *32*, 15–45. [[CrossRef](#)]
4. Rawat, I.; Ranjith Kumar, R.; Mutanda, T.; Bux, F. Biodiesel from microalgae: A critical evaluation from laboratory to large scale production. *Appl. Energy* **2013**, *103*, 444–467. [[CrossRef](#)]
5. Cole, A.J.; Neveux, N.; Whelan, A.; Morton, J.; Vis, M.; de Nys, R.; Paul, N.A. Adding value to the treatment of municipal wastewater through the intensive production of freshwater macroalgae. *Algal Res.* **2016**, *20*, 100–109. [[CrossRef](#)]
6. Lawton, R.J.; Cole, A.J.; Roberts, D.A.; Paul, N.A.; de Nys, R. The industrial ecology of freshwater macroalgae for biomass applications. *Algal Res.* **2017**, *24*, 486–491. [[CrossRef](#)]
7. Neveux, N.; Magnusson, M.; Maschmeyer, T.; de Nys, R.; Paul, N.A. Comparing the potential production and value of high-energy liquid fuels and protein from marine and freshwater macroalgae. *GCB Bioenergy* **2014**, *7*, 673–689. [[CrossRef](#)]
8. Zeraatkar, A.K.; Ahmadzadeh, H.; Talebi, A.F.; Moheimani, N.R.; McHenry, M.P. Potential use of algae for heavy metal bioremediation, a critical review. *J. Env. Manag.* **2016**, *181*, 817–831. [[CrossRef](#)]
9. Castine, S.A.; Paul, N.A.; Magnusson, M.; Bird, I.; de Nys, R. Algal bioproducts derived from suspended solids in intensive land-based aquaculture. *Bioresour. Technol.* **2013**, *131*, 113–120. [[CrossRef](#)]
10. Lawton, R.J.; Mata, L.; de Nys, R.; Paul, N.A. Algal bioremediation of waste waters from land-based aquaculture using *Ulva*; selecting target species and strains. *PLoS ONE* **2013**, *8*, e77344. [[CrossRef](#)]
11. Machado, L.; Kinley, R.; Magnusson, M.; de Nys, R.; Tomkins, N. The potential of macroalgae for beef production systems in Northern Australia. *J. Appl. Phycol.* **2015**, *27*, 2001–2005. [[CrossRef](#)]
12. Machado, L.; Magnusson, M.; Paul, N.; Kinley, R.; de Nys, R.; Tomkins, N. Dose-response effects of *asparagopsis taxiformis* and *oedogonium* sp. on in vitro fermentation and methane production. *J. Appl. Phycol.* **2016**, *28*, 1443–1452. [[CrossRef](#)]
13. Show, K.; Lee, D.; Chang, J. Algal biomass dehydration. *Bioresour. Technol.* **2013**, *135*, 720–729. [[CrossRef](#)] [[PubMed](#)]
14. Henderson, S.M.; Pabis, S. Grain drying theory I: Temperature effects on drying coefficients. *J. Agric. Eng. Res.* **1961**, *6*, 169–174.
15. Moreira, R.; Chenlo, F.; Sineiro, J.; Arufe, S.; Sexto, S. Water sorption isotherms and air drying kinetics of *fucus vesiculosus* brown seaweed. *J. Food Process. Preserv.* **2017**, *41*, e12997. [[CrossRef](#)]
16. Vega-Gálvez, A.; Ayala-Aponte, A.; Notte, E.; Fuente, L.; Lemus-Mondaca, R. Mathematical Modeling of Mass Transfer during Convective Dehydration of Brown Algae *Macrocystis Pyrifera*. *Dry. Technol.* **2008**, *26*, 1610–1616. [[CrossRef](#)]
17. Djaeni, M.; Sari, D.A. Low temperature seaweed drying using dehumidified air. *Procedia Env. Sci.* **2015**, *23*, 2–10. [[CrossRef](#)]
18. Uribe, E.; Vega-Gálvez, A.; Vásquez, V.; Lemus-Mondaca, R.; Callejas, L.; Pastén, A. Hot-air drying characteristics and energetic requirement of the edible brown seaweed *Durvillaea antarctica*. *J. Food Process. Preserv.* **2017**, *41*, e13313. [[CrossRef](#)]
19. Gupta, S.; Cox, S.; Abu-Ghannam, N. Effect of different drying temperatures on the moisture and phytochemical constituents of edible Irish brown seaweed. *Food Sci. Technol.* **2011**, *44*, 1266–1272. [[CrossRef](#)]
20. Oliveira, E.; Rosa, G.; Moraes, M.; Pinto, L. Characterization of thin layer drying of *spirulina platensis* utilizing perpendicular air flow. *Bioresour. Technol.* **2009**, *100*, 1297–1303. [[CrossRef](#)]
21. Dissa, O.; Compaore, A.; Tiendrebeogo, E.; Kouliadiati, J. An effective moisture diffusivity model deduced from experiment and numerical solution of mass transfer equations for a shrinkable drying slab of microalgae *spirulina*. *Dry. Technol.* **2014**, *32*, 1231–1244. [[CrossRef](#)]
22. Fick, A.V. On liquid diffusion. *Philos. Mag.* **1855**, *10*, 30–39. [[CrossRef](#)]
23. Sherwood, T.K. The drying of solids—I. *Ind. Eng. Chem.* **1932**, *24*, 307–310. [[CrossRef](#)]
24. Lemus, R.A.; Pérez, M.; Andrés, A.; Roco, T.; Tello, C.M.; Vega, A. Kinetic study of dehydration and desorption isotherms of red alga *Gracilaria*. *Food Sci. Technol.* **2008**, *41*, 1592–1599. [[CrossRef](#)]
25. Anderson, R.B. Modifications of the Brunauer, Emmett and Teller equation. *J. Am. Chem. Soc.* **1946**, *68*, 686–691. [[CrossRef](#)]
26. Guillard, V.; Bourlieu, C.; Gontard, N. *Food Structure and Moisture Transfer: A Modelling Approach*; Springer: New York, NY, USA, 2013. [[CrossRef](#)]

27. Neveux, N.; Yuen, A.K.L.; Jazrawi, C.; Magnusson, M.; Haynes, B.S.; Masters, A.F.; Montoya, A.; Paul, N.A.; Maschmeyer, T.; de Nys, R. Biocrude yield and productivity from the hydrothermal liquefaction of marine and freshwater green macroalgae. *Bioresour. Technol.* **2014**, *155*, 334–341. [[CrossRef](#)]
28. Lawton, R.J.; de Nys, R.; Paul, N.A. Selecting reliable and robust freshwater macroalgae for biomass applications. *PLoS ONE* **2013**, *8*, e64168. [[CrossRef](#)]
29. Vucko, M.; Cole, A.; Moorhead, J.; Pit, J.; de Nys, R. The freshwater macroalga *Oedogonium intermedium* can meet the nutritional requirements of the herbivorous fish *Ancistrus cirrhosus*. *Algal Res.* **2017**, *27*, 21–31. [[CrossRef](#)]
30. Greenspan, L. Humidity set points of binary aqueous solutions. *J. Res. Natl. Inst. Stand. Technol.* **1976**, *81*, 89–96. [[CrossRef](#)]
31. Walker, C.; Cole, A.; Sheehan, M. Modelling of thin layer drying of macroalgae. Presetend at the Asia Pacific Confederation of Chemical Engineering Congress 2015, Melbourne, Australia, 27 September–1 October 2015.
32. Mohamed, L.A.; Kouhila, M.; Lahsasni, S.; Jamali, A.; Idlimam, A.; Rhazi, M.; Aghfir, M.; Mahrouz, M. Equilibrium moisture content and heat of sorption of *Gelidium sesquipedale*. *J. Stored Prod. Res.* **2005**, *41*, 199–209. [[CrossRef](#)]
33. Al-Muhtaseb, A.H.; McMinn, W.A.M.; Magee, T.R.A. Moisture sorption isotherm characteristics of food products: A review. *Food Bioprod. Process.* **2002**, *80*, 118–128. [[CrossRef](#)]
34. Kiranoudis, C.; Tsami, E.; Maroulis, Z.; Marinou-Kouris, D. Drying kinetics of some fruits. *Dry. Technol.* **1997**, *15*, 1399–1418. [[CrossRef](#)]
35. Moussaoui, H.; Bahammou, Y.; Idlimam, A.; Lamharrar, A.; Abdenouri, N. Investigation of hygroscopic equilibrium and modeling sorption isotherms of the argan products: A comparative study of leaves, pulps, and fruits. *Food Bioprod. Process.* **2019**, *114*, 12–22. [[CrossRef](#)]
36. Zomorodian, A.; Kavooosi, Z.; Momenzadeh, L. Determination of EMC isotherms and appropriate mathematical models for canola. *Food Bioprod. Process.* **2011**, *89*, 407–413. [[CrossRef](#)]
37. Xanthopoulos, G.; Yanniotis, S.; Lambrinos, G.R. Water diffusivity and drying kinetics of air drying of figs. *Dry. Technol.* **2009**, *27*, 502–512. [[CrossRef](#)]
38. Cárcel, J.; García-Pérez, J.; Riera, E.; Mulet, A. Influence of high intensity ultrasound on drying kinetics of persimmon. *Dry. Technol.* **2007**, *25*, 185–193. [[CrossRef](#)]
39. Santacatalina, J.; Soriano, J.; Cárcel, J.; Garcia-Perez, J. Influence of air velocity and temperature on ultrasonically assisted low temperature drying of eggplant. *Food Bioprod. Process.* **2016**, *100*, 282–291. [[CrossRef](#)]
40. Hassini, L.; Azzouz, S.; Peczalski, R.; Belghith, A. Estimation of potato moisture diffusivity from convective drying kinetics with correction for shrinkage. *J. Food Eng.* **2007**, *79*, 47–56. [[CrossRef](#)]
41. Krokida, M.; Karathanos, V.; Maroulis, Z.; Marinou-Kouris, D. Drying kinetics of some vegetables. *J. Food Eng.* **2003**, *59*, 391–403. [[CrossRef](#)]
42. Scala, K.; Crapiste, G. Drying kinetics and quality changes during drying of red pepper. *Food Sci. Technol.* **2008**, *41*, 789–795. [[CrossRef](#)]
43. Rosa, D.; Cantú-Lozano, D.; Luna-Solano, G.; Polachini, T.; Telis-Romero, J. Mathematical modeling of orange seed drying kinetics. *Ciênc. Agrotecnol.* **2015**, *39*, 291–300. [[CrossRef](#)]

